

Elaboration of superparamagnetic nanorods using iron oxide nanoparticles and polymers

J. Fresnais^{*}, J.-F. Berret^{*@}, B. Frka-Petecic^{**}, O. Sandre^{**} and R. Perzynski^{**}

^{*} : Matière et Systèmes Complexes, UMR 7057 CNRS Université Denis Diderot Paris-VII, Bâtiment Condorcet, 10 rue Alice Domon et Léonie Duquet, 75205 Paris, France

^{**} Laboratoire Liquides Ioniques et Interfaces Chargées, UMR 7612 CNRS Université Pierre et Marie Curie Paris-VI, 4 place Jussieu, F-75252 Paris Cedex 05 France

ABSTRACT

During the past years, we have investigated the complexation between metal oxide nanoparticles and oppositely charged polymers. The attractive interactions between oppositely charged species are strong and in general the simple mixing of disperse solutions results in a precipitation, or in a phase separation. Recently, we have developed means to control the electrostatically-driven attractions and at the same time to preserve the stability of the dispersions. Using this approach we have designed novel nanostructures, as those obtained with iron and cerium oxide nanoparticles. In this presentation, we give an account of the formation of colloidal and supracolloidal aggregates obtained by controlled co-assembly of 7 nm particles with copolymers. Nanostructured rods of length comprised between 1 and 100 μm and diameter 500 nm were also disclosed. By application of an external magnetic field, the nanorods were found to reorient along with the magnetic field axis. Preliminary micro-rheology experiments on test fluids have demonstrated the potential use of these nanostructured rods to determine the local viscosity of fluids.

@ : jean-francois.berret@univ-paris-diderot.fr

Keywords: iron oxide - nanoparticles – superparamagnetic nanorods – block copolymers

1 INTRODUCTION

Since the pioneering works by Kataoka and Harada [1,2], it has been recognized that attractive interactions between polyelectrolyte-neutral diblock copolymers and oppositely charged species result in the formation of new type of colloids. These colloids form spontaneously by electrostatic self-assembly with a core-corona microstructure. With polyelectrolyte-neutral copolymers, the complexation is controlled by the appropriate choice of the polymer, its molecular weight and by the molecular weight ratio between the two blocks.

Optimum conditions for complexation have been determined experimentally. These conditions are reached

when the degree of polymerization of the neutral block is 2 - 5 times that of the charged block. So far, the specimens examined with respect to copolymer complexation comprise synthetic [3] and biological [1] macromolecules, multivalent counterions [4,5], surfactant micelles [6-10]. The formation of the mixed aggregates is generally understood as the result of a nucleation and growth mechanism of a microphase made from the oppositely charged constituents. This growth is arrested at a size which is fixed by the dimension of the polymer, i.e. the range 20 – 100 nm.

In this extended abstract, we report that the electrostatic complexation is effective too, using crystalline nanoparticles of size less than 10 nm [11-14]. We have investigated anionically modified dispersions of iron oxide particles stabilized by poly(acrylic acid) [15,16]. By combining an appropriate choice of copolymer [17,18] and of kinetics of association, we are able to assemble the particles into spherical or cylindrical aggregates in the micrometer range. We show that the particles are aggregated in densely packed state with internal volume fraction of 25 % . For the elongated aggregates, also called nanorods, we also derive the probability distribution functions of length and discuss their mechanisms of reorientations under the application of a magnetic field.

2 EXPERIMENTAL

2.1 Polymers

The anionically charged nanoparticles have been complexed with a cationic-neutral diblock copolymer, referred to as poly(trimethylammonium ethylacrylate)-*b*-poly(acrylamide) (Fig. 1). The counterion associated with the quaternary ammonium group was methyl sulfate. The diblock copolymers were synthesized by MADIX® controlled radical polymerization which is a Rhodia patented process [19,20]. The molecular weight put under scrutiny in this study corresponds to $m = 41$ monomers in the charged blocks ($M_w = 11\,000\text{ g}\cdot\text{mol}^{-1}$) and $n = 420$ for the neutral chain ($M_w = 30\,000\text{ g}\cdot\text{mol}^{-1}$). In accordance with previous reports [8-10], the copolymer was abbreviated PTEA_{11K}-*b*-PAM_{30K}. In aqueous solutions at

neutral pH, the chains are dispersed and in the state of unimers. Light scattering performed in the dilute regime have revealed a molecular weight $M_w = 35\,000 \pm 2000\text{ g mol}^{-1}$ and an hydrodynamic diameter $D_H = 11 \pm 1\text{ nm}$ [8]. The polydispersity index was determined by size exclusion chromatography at 1.6. In case of one-shot direct mixing between polymers and particles [11,17], the role of the neutral chains was to restrain a coacervate microphase separation at the 100 nm scale.

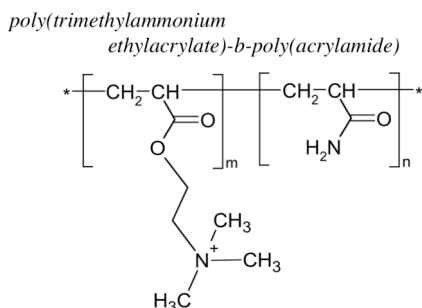


Figure 1 : Chemical structure of the diblock copolymer PTEA-*b*-PAM investigated in the present work, with $m = 41$ and $n = 420$. The abbreviation PTEA stands for poly(trimethylammonium ethylacrylate methylsulfate) and PAM for poly(acrylamide).

2.2 Iron Oxide Nanoparticles

The synthesis of magnetic nanoparticles investigated here was elaborated by R. Massart three decades ago using the technique of « soft chemistry » [21]. This technique is based on the polycondensation of metallic salts in alkaline aqueous media, resulting in the formation of magnetite (Fe_3O_4) nanoparticles of sizes comprised between 4 and 15 nm. In a second stage, magnetite was further oxidized into maghemite ($\gamma\text{-Fe}_2\text{O}_3$) and the nanoparticles were sorted according to their size. Fig. 2 displays typical transmission electron cryo-microscopy (cryo-TEM) images of $\gamma\text{-Fe}_2\text{O}_3$ nanoparticles [11].

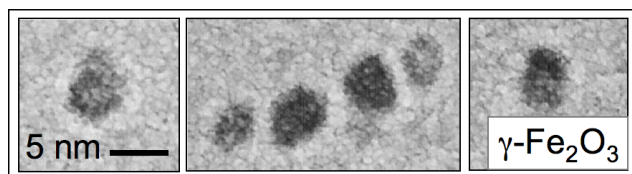


Figure 2 : Iron oxide nanoparticles as observed by transmission electron cryo-microscopy [11]. The stability of the dispersions is ensured by electrostatic interactions mediated by ligands or oligomers adsorbed on their surface.

These dispersions have been studied thoroughly with respect to several fundamental properties, including *i*) the control of the size distribution [22], *ii*) the colloidal stability and the modification of the surface chemistry of the particles [23] and *iii*) the magnetic birefringence and giant

paramagnetism, which described the behavior of the particles in magnetic field and gradients [24].

In the conditions of the synthesis (pH 1.8, weight concentration $c = 6.58\text{ wt. \%}$, volume fraction of $\phi = 1.29\%$), the magnetic dispersions were thermodynamically stable over a period of years. They were stabilized by electrostatic interactions arising from the native cationic charges at the surface of the particles. Nitrate ions served as counterions and insure electroneutrality. We refer to Refs. [11,12,16,23,24] for further reading.

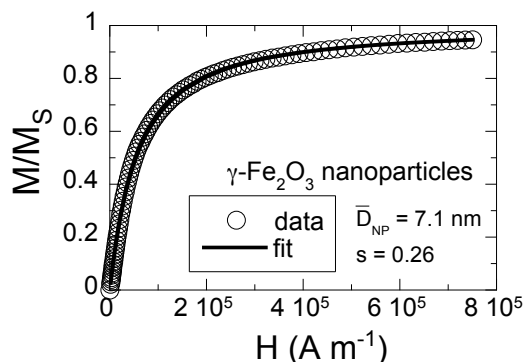


Figure 3 : Magnetic field dependence of the macroscopic magnetization $M(H)$ normalized by its saturation value M_S for cationic maghemite dispersions. The solid curve was obtained using the Langevin function for paramagnetism convoluted with a log-normal distribution function for the particle sizes.

Vibrating sample magnetometry consisted in measuring the magnetization versus excitation $M(H)$ for a solution at volume fraction ϕ . Fig. 3 shows the evolution of the macroscopic magnetization $M(H)$ normalized by its saturation value M_S for the present $\gamma\text{-Fe}_2\text{O}_3$ batch. Here, $M_S = \phi m_s$, where m_s the volumetric magnetization of maghemite ($m_s = 2.6 \times 10^5\text{ A m}^{-1}$). The solid curve in Fig. 3 was obtained using the Langevin function for paramagnetism convoluted with a log-normal distribution function of the particle size. The parameters of the distribution are the median diameter $7.1 \pm 0.3\text{ nm}$ and the polydispersity of 0.26 ± 0.03 . The polydispersity is defined as the ratio between the standard deviation and the average diameter. With dynamic light scattering, a single mode in the autocorrelation function was observed, corresponding to an hydrodynamic diameter $D_H = 14 \pm 1\text{ nm}$ and a polydispersity index of 0.12.

2.3 Optical microscopy

Phase-contrast images of the nanorods were acquired on a IX71 inverted microscope (Olympus, Rungis, France) equipped with a 100X objective. We used a Photometrics Cascade camera (Roper Scientific, Evry, France) and Metaview software (Universal Imaging Inc.). For the

observations of the reorientations under external magnetic field, we used a Leitz (Ortholux) upward microscope with a $\times 20$ objective. The magnetic field was applied using two pairs of coils orthogonal to each other [25]. A nanorod was selected and oriented by the first pair of coils by an AC current operating at 10 Hz. Once aligned, this primary field was removed and the rod was let free to move by Brownian motions for a couple of seconds. Doing so, the rods were slightly misaligned, with an angle θ_0 comprised between 80° to 87° . We recall that θ denotes the angle between the major axis of a rod and the Y-direction. A DC current was then applied on the perpendicular coils along the Y-direction by a power supplied generator. As a result, the rods rotated in the plane of observation from θ_0 to 0° . In this configuration, the experiments were carried out at different values of the magnetic field, between $10^3 - 10^4$ A m^{-1} . Video sequences were recorded by a CCD camera, digitized and treated by the ImageJ software. Movies of rod reorientations are shown in Supporting Information.

3 RESULTS

The superparamagnetic nanorods were obtained from mixing the 7 nm magnetic nanoparticles and the polymers of appropriate molecular weight, in a process that will be described in a forthcoming paper.

Fig. 3a shows an image ($\times 100$) of a nanorod dispersion sealed between glass plates. Elongated structures were clearly visible, with typical sizes in the micrometer range. For this specimen, image analysis has allowed to derive the length distribution of the rods. Fig. 4 displays the length distribution of the nanorods observed by microscopy on a series of images. The statistics was acquired on 116 specimens, yielding a distribution that was centered around 10 μm . The data could be conveniently fitted using a log-normal function with median length $L_{Rod} = 12.3 \pm 0.7 \mu m$, and a polydispersity $s = 0.55$. It is important to note that the nanorods did not display signs of destabilization (neither flocculation nor degradation), even after several months. As shown in Fig. 3a, the nanorods were randomly oriented in absence of magnetic field. However, if a magnet was brought near to the cell, the rods reoriented spontaneously and followed the external magnetic field. Fig. 3b and 3c illustrate orientations in the plane of the figure and perpendicular to it, respectively. The origin of magnetic coupling is examined below.

We here demonstrate that the rods have inherited the properties of the nanoparticles, namely to be superparamagnetic [12,13]. Superparamagnetic implies that the rods do not carry a permanent magnetic moment (an indication is provided by the randomly distributed orientations in absence of field), but acquire one under the application of a field. We have performed quantitative measurements of the kinetics associated with reorientations.

Let us denote by $\theta(t)$ the angle between the major axis of a rod and applied excitation H.

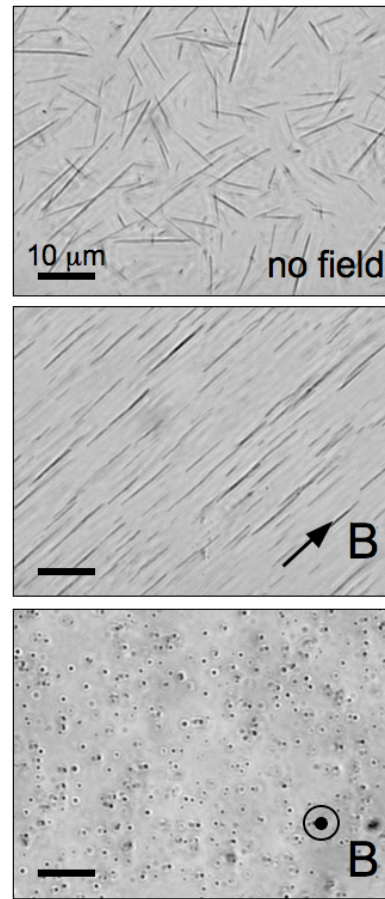


Figure 4 : Phase contrast optical microscopy images ($\times 100$) of a nanorod dispersion without magnetic field (a), with the magnetic field applied perpendicular (b) and parallel (c) to the optical axis of the microscope. The dots in c) display the nanorods seen from above. For this dispersion, the average length of the rods was found to be 12.3 μm , and the polydispersity $s = 0.50$.

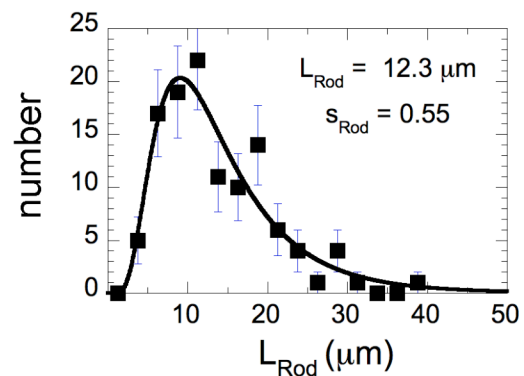


Figure 5 : Length distribution of nanorods in Fig. 3. The continuous line was derived from best fit calculation using a log-normal distribution.

At the application of an external field at 90° with respect to the initial conditions, the nanorods rotated in the plane of observation around their center of gravity, in a propeller-like motion. The reorientational dynamics results from the balance between the magnetic torque and the hydrodynamic drag [25,26], yielding an expression of the form :

$$\operatorname{tg} \theta(t) = \operatorname{tg} \theta_0 \exp(-kt) \quad (1)$$

In Eq. 3a, θ_0 was the initial position of the rods prior to the application of the field and k the decay rate of the reorientation. k depends on the geometrical parameters of the rods, such as the length and diameter, and on the strength of the applied field. All experiments were then performed with $\theta_0 = 80 - 87^\circ$ using a procedure described in the experimental section. Fig. 6 illustrates the time dependence of $\operatorname{tg} \theta(t)$ for a rod of length $12 \mu\text{m}$. The semilogarithmic representation was implemented in order to emphasize the exponential character of the reorientation towards $\theta = 0^\circ$. The good agreement between the experimental data and the predictions of Eq. 1 (straight line in Fig. 6) attests of the reliability of the model.

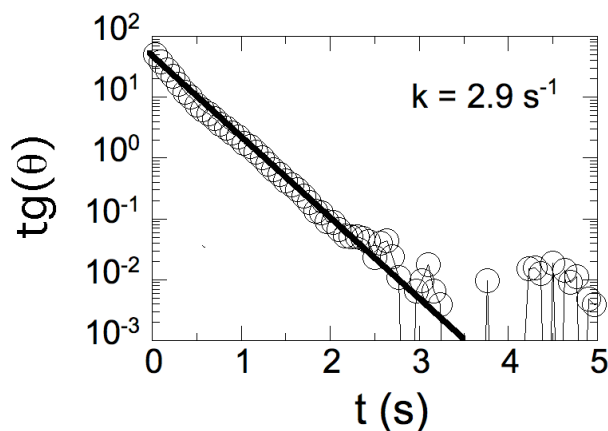


Figure 6 : Tangent of the reorientation angle $\theta(t)$ as a function of the time. The parameter k for this set of data was $k = 2.9 \text{ s}^{-1}$. Note that the exponential decay was observed over 4 decades in the ordinate units.

4 CONCLUSION

In conclusion, we have shown that the electrostatic interactions between oppositely charged magnetic nanoparticles and polymers can be accurately controlled. Under appropriate conditions, this control resulted in the fabrication of elongated aggregates which display remarkable stiffness and magnetic properties.

REFERENCES

- [1] K. Kataoka; H. Togawa; A. Harada; K. Yasugi; T. Matsumoto; S. Katayose. *Macromolecules* 29 (1996) 8556 .
 [2] A. Harada; K. Kataoka. *Science* 283 (1999) 65 .

- [3] S.v.d. Burgh; R. Fokkink; A.d. Keizer; M.A.C. Stuart. *Colloids and Surfaces A - physicochemical and Engineering Aspects* 242 (2004) 167 .
 [4] E. Raspaud; M. Olvera-de-la-Cruz; J.-L. Sikorav; F. Livolant. *Biophys. J.* 74 (1998) 381 .
 [5] F. Bouyer; C. Gérardin; F. Fajula; J.-L. Puteaux; T. Chopin. *Colloids Surf. A* 217 (2003) 179 .
 [6] J.-F. Berret; G. Cristobal; P. Herve; J. Oberdisse; I. Grillo. *European Physical Journal E* 9 (2002) 301 .
 [7] P. Herve; M. Destarac; J.-F. Berret; J. Lal; J. Oberdisse; I. Grillo. *Europhysics Letters* 58 (2002) 912 .
 [8] J.-F. Berret; P. Herve; O. Aguerre-Chariol; J. Oberdisse. *Journal of Physical Chemistry B* 107 (2003) 8111 .
 [9] J.-F. Berret; B. Vigolo; R. Eng; P. Herve; I. Grillo; L. Yang. *Macromolecules* 37 (2004) 4922 .
 [10] J.-F. Berret. *Journal of Chemical Physics* 123 (2005) .
 [11] J.-F. Berret; A. Sehgal; M. Morvan; O. Sandre; A. Vacher; M. Airiau. *Journal of Colloid and Interface Science* 303 (2006) 315 .
 [12] J.-F. Berret; N. Schonbeck; F. Gazeau; D. El Kharrat; O. Sandre; A. Vacher; M. Airiau. *Journal of the American Chemical Society* 128 (2006) 1755 .
 [13] J.-F. Berret. *Macromolecules* 40 (2007) 4260 .
 [14] L. Qi; J.P. Chapel; J.C. Castaing; J. Fresnais; J.-F. Berret. *Langmuir* 23 (2007) 11996 .
 [15] A. Sehgal; Y. Lalatonne; J.-F. Berret; M. Morvan. *Langmuir* 21 (2005) 9359 .
 [16] J.-F. Berret; O. Sandre; A. Mauger. *Langmuir* 23 (2007) 2993 .
 [17] K. Yokota; M. Morvan; J.-F. Berret; J. Oberdisse. *Europhysics Letters* 69 (2005) 284 .
 [18] J.-F. Berret; K. Yokota; M. Morvan; R. Schweins. *Journal of Physical Chemistry B* 110 (2006) 19140 .
 [19] M. Destarac; W. Bzducha; D. Taton; I. Gauthier-Gillaizeau; S.Z. Zard. *Macromol. Rapid Commun.* 23 (2002) 1049 .
 [20] M. Jacquín; P. Muller; G. Lizarraga; C. Bauer; H. Cottet; O. Théodoly. *Macromolecules* 40 (2007) 2672 .
 [21] R. Massart; E. Dubois; V. Cabuil; E. Hasmonay. *J. Magn. Magn. Mat.* 149 (1995) 1 .
 [22] A. Bee; R. Massart; S. Neveu. *J. Magn. Magn. Mat.* 149 (1995) 6 .
 [23] E. Dubois; V. Cabuil; F. Boue; R. Perzynski. *J. Chem. Phys.* 111 (1999) 7147 .
 [24] E. Hasmonay; E. Dubois; J.-C. Bacri; R. Perzynski; Y.L. Raikher; V.I. Stepanov. *Eur. J. Phys. B* 5 (1998) 859 .
 [25] D. Letellier; O. Sandre; C. Menager; V. Cabuil; M. Lavergne. *Materials Science & Engineering C-Biomimetic and Supramolecular Systems* 5 (1997) 153 .
 [26] A. Anguelouch; R.L. Leheny; D.H. Reich. *Applied Physics Letters* 89 (2006) 111914 .